HFSE-enriched Metamorphic Blue Sapphires: FTIR and Trace-element Study, and Implications for Heat-Treatment Detection

Michael S. Krzemnicki, Laurent E. Cartier, Wei Zhou, Pierre Lefèvre, Markus Wälle, Hao A. O. Wang and Judith Braun

ABSTRACT: This study examines sapphires naturally enriched in high-field-strength elements (HFSE) from metamorphic origins in Sri Lanka and Madagascar. These sapphires display distinctive chemical inhomogeneities and microscopic growth features, as well as variable FTIR spectra, often including a broad absorption band near 3300 cm^{-1}. Some of the studied samples also show FTIR spectral characteristics and short-wave UV luminescence typically associated with heat-treated stones, although all were unheated. Our findings demonstrate that commonly used indicators—such as specific FTIR band patterns (mainly the 3309 cm^{-1} triplet) and chalky bluish white short-wave UV fluorescence—are not always reliable for identifying heat treatment. Accurate distinction between heated and unheated sapphires requires detailed microscopic examination combined with advanced trace-element analysis and spectroscopic techniques, including Raman micro-spectroscopy of inclusions such as zircon, goethite and diaspore.

The Journal of Gemmology, **40**(2), 2026, pp. 142–156, https://doi.org/10.15506/JoG.2026.40.2.142

The chemical composition of gem materials—particularly their trace-element signatures—reflects their geological formation conditions. This includes gem corundum (Al_2O_3). However, due to its dense crystal structure, corundum accommodates significantly fewer chemical impurities than minerals with larger-spaced crystal lattices, such as tourmaline or beryl. Among gem corundum, blue sapphires occur in a wide range of geological environments, and are commonly classified, from a geological perspective, into metamorphic (e.g. granulite- or amphibolite-related) and magmatic (e.g. alkali basalt-related) types (e.g. Giuliani *et al*. 2014). This distinction is based not only on their host rocks and formation processes, but also on characteristic trace-element patterns and spectroscopic features, which are widely used in gem testing to determine geographic origin.

A particular subset of metamorphic sapphires forms through metasomatic fluid activity. This includes those from skarn-related deposits (e.g. from Andranondambo in southern Madagascar; Schwarz *et al*. 1996; Gübelin & Peretti 1997), as well as sapphires formed by fluid-driven processes during large-scale orogenic events and metamorphism (e.g. from Afghanistan [Dutrow *et al*. 2019], the southern Andes [Miranda-Díaz *et al*. 2022] and Sri Lanka [Pannipitiye *et al*. 2012]). Such sapphires are often characterised by elevated Ti contents, as well as the presence of other 'exotic' elements—known as high-field-strength elements (HFSE)—such as Zr, Nb, Sn, Hf, Ta, W and Th. These sapphires are of particular interest in gemmological

Figure 1: A selection of the unheated HFSE-enriched sapphires (5.68–20.23 ct) from Madagascar and Sri Lanka used in this study shows the quality and sizes in which this type of sapphire can occur. Photos by L. Phan, SSEF; digitally arranged by M. S. Krzemnicki.

research because HFSE concentrations frequently correlate with the presence of naturally incorporated Be (Wathanakul *et al*. 2004, 2007; Krzemnicki *et al*. 2007; Pardieu 2007, 2013; Shen *et al*. 2007; Pardieu & Klemm 2008; Pardieu *et al*. 2011; Saeseaw *et al*. 2017). This provides a robust criterion for distinguishing unheated sapphires containing natural traces of Be from those subjected to Be-diffusion treatment, which do not exhibit a correlation between HFSE and Be. Furthermore, some HFSE-bearing sapphires contain measurable amounts of Th and Pb, enabling direct radiometric age determination (Krzemnicki *et al*. 2019; Wang *et al*. 2019; Wälle & Wang 2023; Zhou *et al*. 2024).

Building upon initial results presented by Krzemnicki *et al*. (2025b), this study characterises HFSE-enriched unheated metamorphic sapphires (e.g. Figure 1)—specifically their internal and spectral features, luminescence to short-wave UV radiation, and trace-element composition—and examines how the presence of HFSE may influence their Fourier-transform infrared (FTIR) spectra, and the implications of this for heat-treatment detection.

BACKGROUND

What Are HFSE and How Are They Incorporated in Sapphires?

The term *high-field-strength elements* refers to chemical elements characterised by a small ionic radius (r) and high ionic charge (Z) with an ionic potential of $Z/r > 2.0$, resulting in a high electrical field strength. Consequently, their bonding to nearby anions is very strong. Typical HFSE include Zr, Nb, Hf and Ta, but also Ti, Sn and Pb, among other elements (see Figure 2).

HFSE are generally considered chemically 'incompatible' elements—that is, ones not easily incorporated into common rock-forming minerals (i.e. silicates).

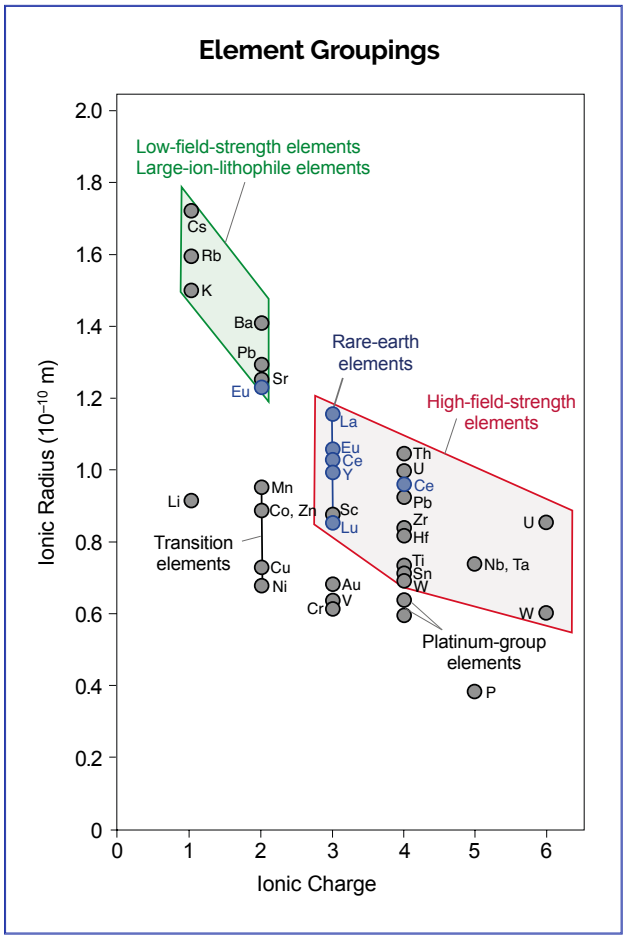

Figure 2: In this plot, elements are grouped based on their ionic charge and ionic radius. High-field-strength elements (HFSE) include rare-earth and other elements with a relatively high ionic charge and small ionic radius, resulting in an ionic potential of >2.0. Adapted from Rollinson (1993) and Jaireth *et al*. (2014).

They tend to be immobile and remain in the residual melt/fluid, in which they may be considerably enriched. However, they can become mobile through chemical complexation with anions such as fluoride (F^-) and hydroxide (OH^-) in hydrothermal and metasomatic fluids. These complexes significantly increase HFSE solubility, with F-rich, Ca-free fluids being particularly effective for transport (Jiang *et al*. 2005).

Interestingly, such 'exotic' trace elements occur in both basaltic sapphires (e.g. from Nigeria, Tasmania and northern Madagascar) and metamorphic sapphires (e.g. from Madagascar, Sri Lanka and Afghanistan), and are commonly associated with metasomatic processes during crystal growth (Upton *et al*. 1999; McGee 2005; Simonet *et al*. 2008; Giuliani *et al*. 2014; Dutrow *et al*. 2019; Miranda-Díaz *et al*. 2022). The incorporation mechanisms of these normally incompatible elements, including Be, have been the subject of several studies. Proposed models suggest either primary entrapment during crystal growth, including the incorporation of nano-inclusions, or direct structural incorporation into the corundum lattice, followed by possible exsolution or epigenetic segregation into nano-clusters or discrete nano-particulate phases (Shen 2011; Shen & Wirth 2012; Oto *et al*. 2023; Emori *et al*. 2024; Jin *et al*. 2024 and references therein).

Prevalence of HFSE-enriched Sapphires

Interestingly, sapphires enriched in HFSE are not uncommon in the gem trade or in those submitted to gemmological laboratories. Because these 'exotic' trace elements do not influence a sapphire's colour or overall quality, the presence of HFSE typically remains undetected without detailed trace-element analysis.

A review of trace-element data collected on blue sapphires over the past decade at SSEF by laser ablation inductively coupled plasma time-of-flight mass spectrometry (LA-ICP-TOF-MS, using our GemTOF instrument) showed that most of them contained only very low concentrations of HFSE—usually limited to sub-ppm levels (Figure 3). However, approximately 30% of the sapphires exhibited distinctly elevated HFSE concentrations, in extreme cases reaching total concentrations of several hundred ppmw.

It should be noted, however, that this apparently high proportion is influenced by analytical bias: (1) only a subset of sapphires submitted to SSEF undergo GemTOF analysis, and (2) trace-element analysis is more frequently applied to those suspected of HFSE enrichment, such as in origin determination studies (e.g. Kashmir vs Madagascar). Thus, we estimate that the true prevalence of HFSE-enriched sapphires in the market is likely lower by a factor of approximately five to ten compared to the dataset presented here. Based on this consideration, we estimate that roughly 3%–6% of gem-quality sapphires currently in the trade may contain elevated HFSE concentrations—although still representing a significant proportion.

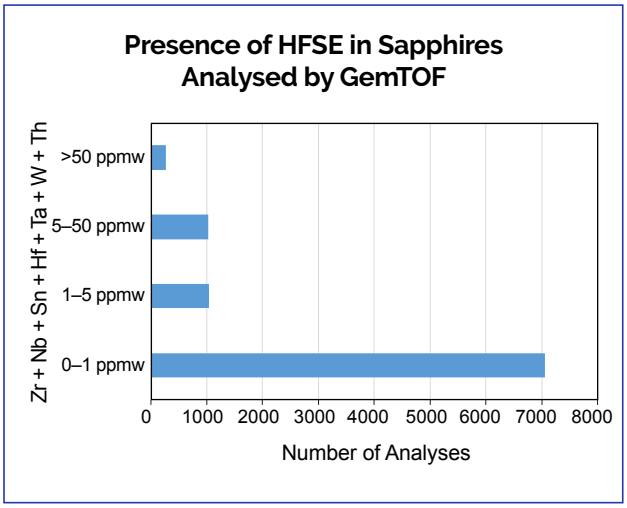

Figure 3: Most of the blue sapphires analysed by SSEF's GemTOF system in the past 10 years have low total concentrations of HFSE (Zr, Nb, Sn, Hf, Ta, W and Th), but some are enriched in HFSE (top three bars). The majority of the sapphires had a metamorphic origin, while about 250 samples were from basaltic/magmatic deposits, and of those about 80 specimens had >1 ppmw HFSE.

MATERIALS & METHODS

For this study, we surveyed more than 100 HFSE-enriched blue sapphires analysed in the past few years at the Swiss Gemmological Institute SSEF. From those, we selected 24 unheated HFSE-enriched sapphires (all containing goethite, diaspore or metamict zircon inclusions) of metamorphic origin (i.e. from Madagascar and Sri Lanka, all supplied by reliable trade members) for an in-depth study. All samples were faceted except for one cabochon (for details, see Table DD-1 in *The Journal*'s online data depository), and some were of large size, ranging up to 20.23 ct. In addition, data from 25 heated metamorphic HFSE-sapphires (also from SSEF's database) were compared with the described unheated samples in this study.

In addition to visual examination and basic gemmological testing of all samples using standard instruments (refractometer and polariscope), micrographs of inclusions were taken using a System Eickhorst Gemmaster trinocular microscope equipped with a Nikon Z 7II camera system. Luminescence to short-wave UV radiation was observed with a UV lamp and/or a DiamondView instrument.

Meticulous Raman spectroscopic analyses were

performed on all 24 sapphires to fully characterise their solid inclusions and to confirm the absence of heat treatment. We used a Renishaw inVia microscope equipped with a Peltier-cooled CCD detector (1024 × 256 pixels), resulting in a maximum spectral resolution of about 1.5 cm^{-1}. The Raman spectra were collected using an argon-ion laser emitting at 514.5 nm. All analyses were carried out in confocal laser mode using the 50× long-working-distance objective of a Leica DM2500 microscope to focus on the inclusions in the sapphires, resulting in a spot size of about 2 µm. We typically used the standard laser power of 35 mW (100% laser emission in our setup, measured on the sample surface), although for goethite analyses the laser power was kept below 3 mW at the sample surface (10% emission) to avoid laser-induced degradation and dehydration effects during analysis (Gialanella *et al*. 2010; Krzemnicki *et al*. 2023). The Raman spectra were accumulated from 10 to 50 spectral scans, and were baseline corrected using Wire software (i.e. integrated cubic-spline baseline function).

Polarised ultraviolet-visible-near infrared (UV-Vis-NIR) absorption spectra were collected from all samples using an Agilent Cary 5000 spectrophotometer (290–900 nm range and 0.35 nm step size). The spectra were all normalised to absorption coefficient (cm^{-1}) to correct for differences in path length.

Unpolarised FTIR spectra were acquired from all samples with a Thermo Scientific Nicolet iS50 spectrometer equipped with a diffuse reflectance accessory (range 6000–400 cm^{-1}, 128 scans and 4 cm^{-1} resolution). Each specimen was measured in at least two orthogonal directions, including the (approximate) direction of the optic axis where possible. For this study, we focused on the mid-FTIR range (3500–3000 cm^{-1}), in which bands related to Ti^{4+}–OH^- complexes occur (e.g. Beran & Rossman 2006) that are often used to separate heated from unheated corundum. FTIR spectra were baseline corrected with Wire software using the cubic-spline function (constructed of third-order polynomials).

To obtain trace-element chemical data, all samples were analysed with SSEF's GemTOF system. The instrumentation employed a 193 nm ArF excimer laser, and was equipped with a TwoVol2 ablation chamber (NWR193UC from Elemental Scientific Lasers, USA) coupled with a commercial ICP-TOF-MS unit (icpTOF from Tofwerk AG, Switzerland), which was modified from an optimised ICP-Q-MS unit (Thermo Scientific iCAP Q). We analysed a minimum of four spots (100 µm diameter) on each sample. All spots were ablated at 20 Hz with a fluence of 5.6 J/cm^2. Helium was used as the carrier gas (0.8–0.9 L/min). Five cleaning laser shots were fired at the beginning of each measurement (30 s ablation time) to remove surface contaminants. We used NIST SRM 610 glass as the external standard and $^{27}Al^+$ (equivalent to 99.8 wt.% Al_2O_3) as an internal standard. Further details of instrumental parameters, analytical conditions, data processing and plotting can be found in Wang *et al*. (2016). In total, 66 elements were analysed for each sample. For this study, we focused on Be, B, Mg, Ti, V, Cr, Fe, Ga, Zr, Nb, Sn, Hf, Ta, W, Pb and Th (see also Table DD-2 in the data depository).

RESULTS AND DISCUSSION

Visual Appearance and Microscopic Features

Most of the HFSE-enriched sapphires showed an attractive velvety appearance due to internal light scattering by sub-microscopic inclusions (Figure 4, left), comparable to that observed in sapphires from Kashmir. However, some lacked turbidity and showed pronounced growth zoning, occasionally with dark grey layers (Figure 4, right).

Viewed with the microscope, the turbidity was seen as areas of milkiness associated with growth zoning or other features (Figure 5). Most of the samples exhibited dense, narrow growth zoning (Figure 5a), produced by subtle oscillatory variations in refractive index, and likely reflecting minor compositional fluctuations during crystal growth. In some cases, this zoning appeared as a more complex, locally 'chaotic' cross-cutting pattern when viewed in certain orientations. The growth zoning was commonly accompanied by pronounced colour zoning, usually manifested as dark ('inky') blue Ti-rich bands (Figure 6). This also included a type of surface-related colour zoning known in the trade by the Ceylonese term *ottu* (Choudhary

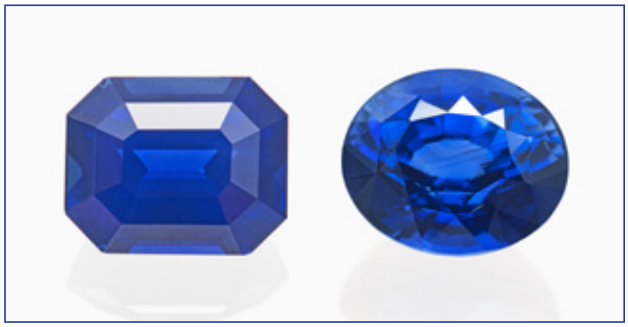

Figure 4: Two unheated sapphires from Madagascar illustrate (left: 13.13 ct, sample S_395) an attractive velvety blue appearance caused by finely dispersed sub-microscopic inclusions, and (right: 12.85 ct, sample S_003) pronounced growth zoning with dark grey layers but almost no turbidity. Both samples are virtually inclusion free and of exceptional gem quality. Photo by A. Chalain, SSEF.

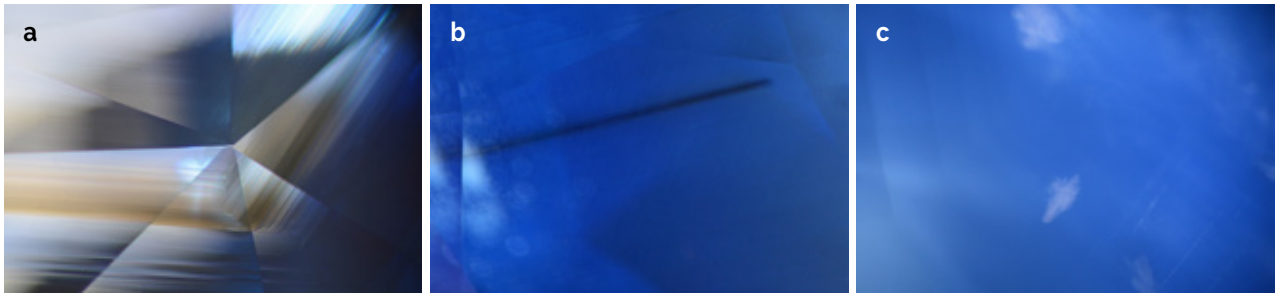

Figure 5: A common characteristic of HFSE-enriched blue sapphires is turbidity. (**a**) Brownish grey turbid layers are associated with growth zoning. (**b**) A linear dark grey zone is made up of accumulations of sub-microscopic particles. (**c**) Milky white turbidity occurs with more-or-less rhombic patches of fine particles. Photomicrographs by M. S. Krzemnicki; magnified 50×.

Figure 6: 'Inky' blue colour zones, narrow growth lines and sector zoning are frequently present in HFSE-enriched sapphires. Photomicrographs by M. S. Krzemnicki; magnified 50×.

2006; Allirol-Mouton *et al*. 2025; Figure 7). Comparable turbidity and colour-zoning features have been described previously, particularly in sapphires from Andranondambo in south-eastern Madagascar (Schwarz *et al*. 1996; Gübelin & Peretti 1997).

The HFSE-enriched sapphires contained relatively few solid inclusions—most commonly zircon (Figure 8a) and graphite. Epigenetic features in some specimens included orange Fe-hydroxide staining along surface-reaching hollow channels and fissures (Figure 8b), as well as colourless acicular crystals of diaspore occurring within fluid inclusions (Figure 9) and along healed fractures.

Raman Micro-spectroscopy

Raman analysis revealed that all 24 sapphires contained hydroxide phases—goethite and/or diaspore—occasionally in association with zircon exhibiting characteristic peak broadening due to metamictisation (Figure 10). Each of these inclusion features

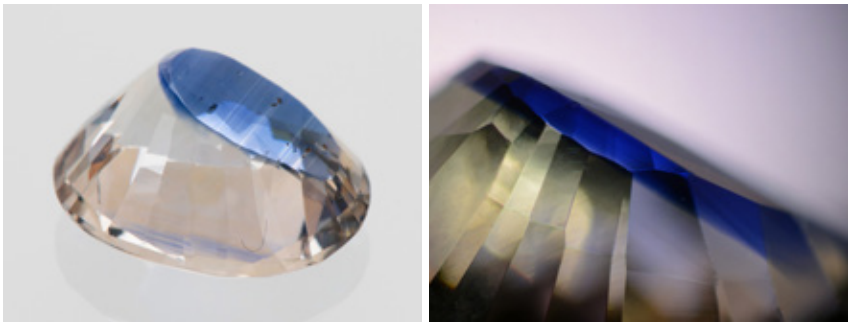

Figure 7: Distinct surface-related colour zoning, known in the trade by the Sri Lankan term *ottu*, can occur in HFSE-enriched sapphires. Photomicrographs by M. S. Krzemnicki; magnified 5× (left) and 50× (right).

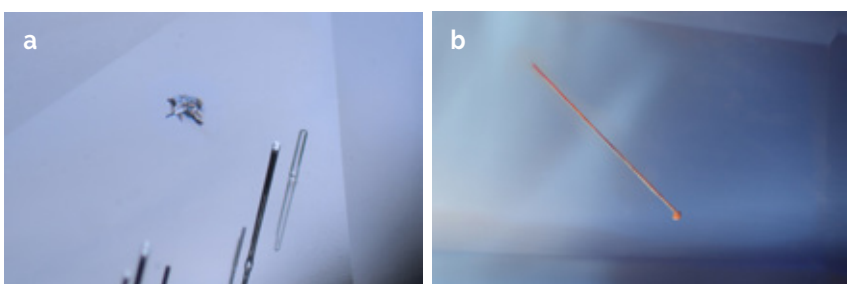

Figure 8: (**a**) A zircon inclusion with tension cracks, together with long-prismatic fluid-bearing tubes, is seen in this HFSE-enriched sapphire. (**b**) Epigenetic features include hollow channels filled with orange Fe-hydroxide. Photomicrographs by M. S. Krzemnicki; magnified 50×.

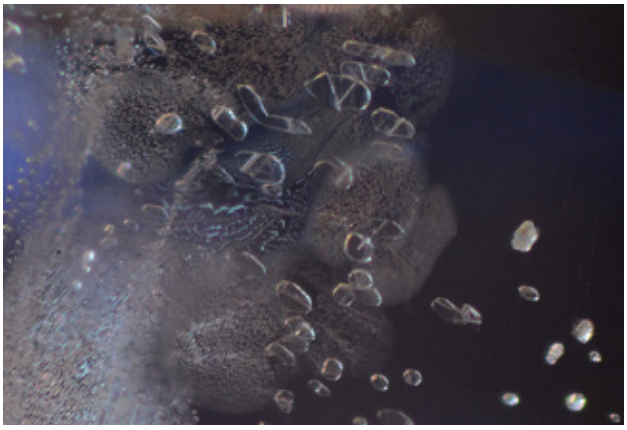

Figure 9: Also present in the HFSE-enriched sapphires are minute colourless diaspore needles within fluid inclusions. Photomicrograph by M. S. Krzemnicki; magnified 70×.

provides confirmation that the sapphires were indeed unheated (see, e.g., Koivula 1987, 2013; Kammerling & Koivula 1989; Nasdala *et al*. 1995; Sripoonjan *et al*. 2016; Karampelas *et al*. 2023; Krzemnicki *et al*. 2023; Curti *et al*. 2025 and references therein).

UV-Vis-NIR Absorption Spectroscopy

The absorption spectra of the metamorphic HFSE-enriched sapphires studied for this report did not show any differences from those of other metamorphic sapphires. They were dominated by a broad band at about 580 nm (Figure 11), attributed to Fe^{2+}–Ti^{4+} intervalence charge transfer and primarily responsible for the blue colouration. Additional Fe-related features occurred at 388 nm (due to isolated Fe^{3+}), and at 377 and 450 nm (corresponding to Fe^{3+}–Fe^{3+} pairs; Dubinsky *et al*. 2020). As in all metamorphic sapphires, the position of the absorption edge in the UV region shifted towards longer wavelengths with increasing turbidity due to the Tyndall effect (Hänni 1994; again, see Figure 11).

Short-wave UV Fluorescence

In this study, we found that natural unheated HFSE-enriched sapphires commonly displayed a 'chalky' bluish white fluorescence under short-wave UV radiation (UV lamp or DiamondView; e.g. Figure 12). In corundum, this short-wave UV response has been mainly attributed to Ti^{4+}-related centres, including octahedral titanate groups (TiO_6) within the crystal lattice (Vigier *et al*. 2023). A similar bluish white fluorescence is also well known in heat-treated corundum, and has been linked to rutile (TiO_2) dissolution and enhanced Ti diffusion into the surrounding lattice (Hughes & Emmett 2005). The fluorescence is typically suppressed by elevated Fe concentrations and is, therefore, absent from Fe-rich magmatic-type sapphires (e.g. from Thailand and Australia; Hughes & Emmett 2005).

In HFSE-enriched sapphires, short-wave UV fluorescence is not heat-treatment related but reflects intrinsic growth conditions associated with metasomatism, which produce pronounced chemical zoning and sectoral variations (Figure 6). As noted above, the unheated nature of all studied samples was previously confirmed by the presence of goethite, diaspore or metamict zircon inclusions (Krzemnicki *et al*. 2023).

Trace-element Composition

In general, the primary defining feature of HFSE-enriched sapphires is their trace-element composition,

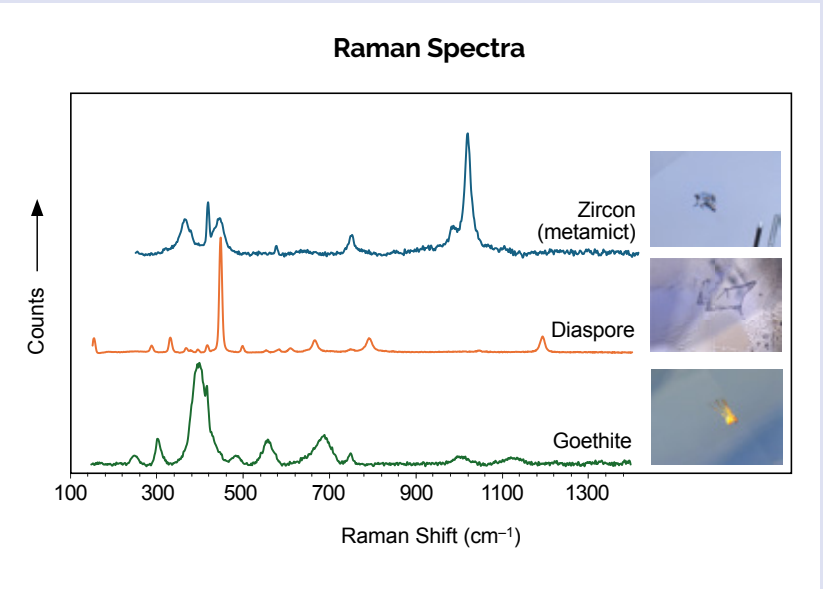

Figure 10: Raman spectra of zircon (with peak broadening due to metamictisation), diaspore and goethite inclusions in HFSE-enriched sapphires confirm that the stones have not been heat treated. The spectra are offset vertically for clarity. Photomicrographs by M. S. Krzemnicki; magnified 80×.

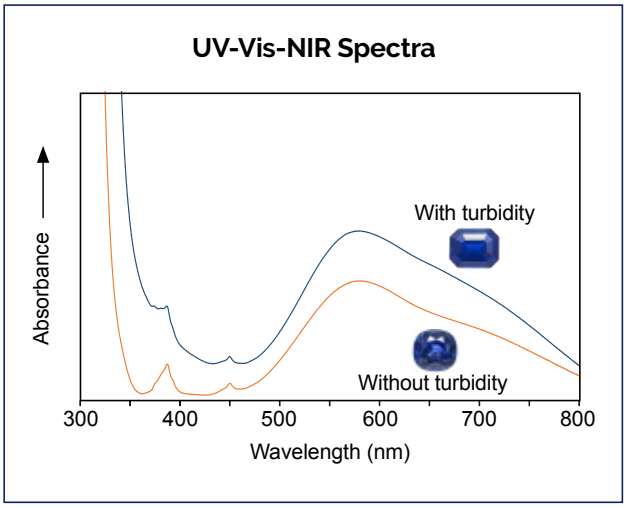

Figure 11: Representative UV-Vis-NIR spectra of two HFSE-enriched sapphires investigated for this study—one with and one without turbidity—demonstrate the shift in the position of the absorption edge that occurs as turbidity increases. The spectra are offset vertically for clarity. Photos by L. Phan, SSEF.

which requires the use of sensitive analytical techniques such as LA-ICP-MS or GemTOF. Based on SSEF's extensive database, most blue metamorphic sapphires contain extremely low HFSE concentrations (commonly below the detection limit), except for Sn, which is typically <1 ppmw. By contrast, in HFSE-enriched sapphires, these impurities range from a few ppmw to several hundred ppmw, occasionally approaching the concentration range of chromophoric elements such as Fe or Ti. In addition, a notable geochemical feature of most HFSE-enriched sapphires is their elevated concentration of Ti compared to Mg, resulting in a high Ti/Mg ratio (typically >>2), as compared to a typical ratio of about 2 in HFSE-poor metamorphic sapphires (Figure 13a). Overall, HFSE concentrations show a broadly positive correlation with Ti (Figure 13b), although this trend can be scattered due to the multi-elemental nature of HFSE. Among plots of individual HFSE pairs, strong positive correlations have been observed for Zr and Hf (Figure 13c) as well as Nb and Ta, reflecting their well-known geochemical coupling due to identical valence states (4+ and 5+, respectively) and nearly identical ionic radii. These element pairs are widely used as petrogenetic tracers (Salters 2016). By contrast, Sn has shown little to no systematic correlation with other HFSE (Figure 13d).

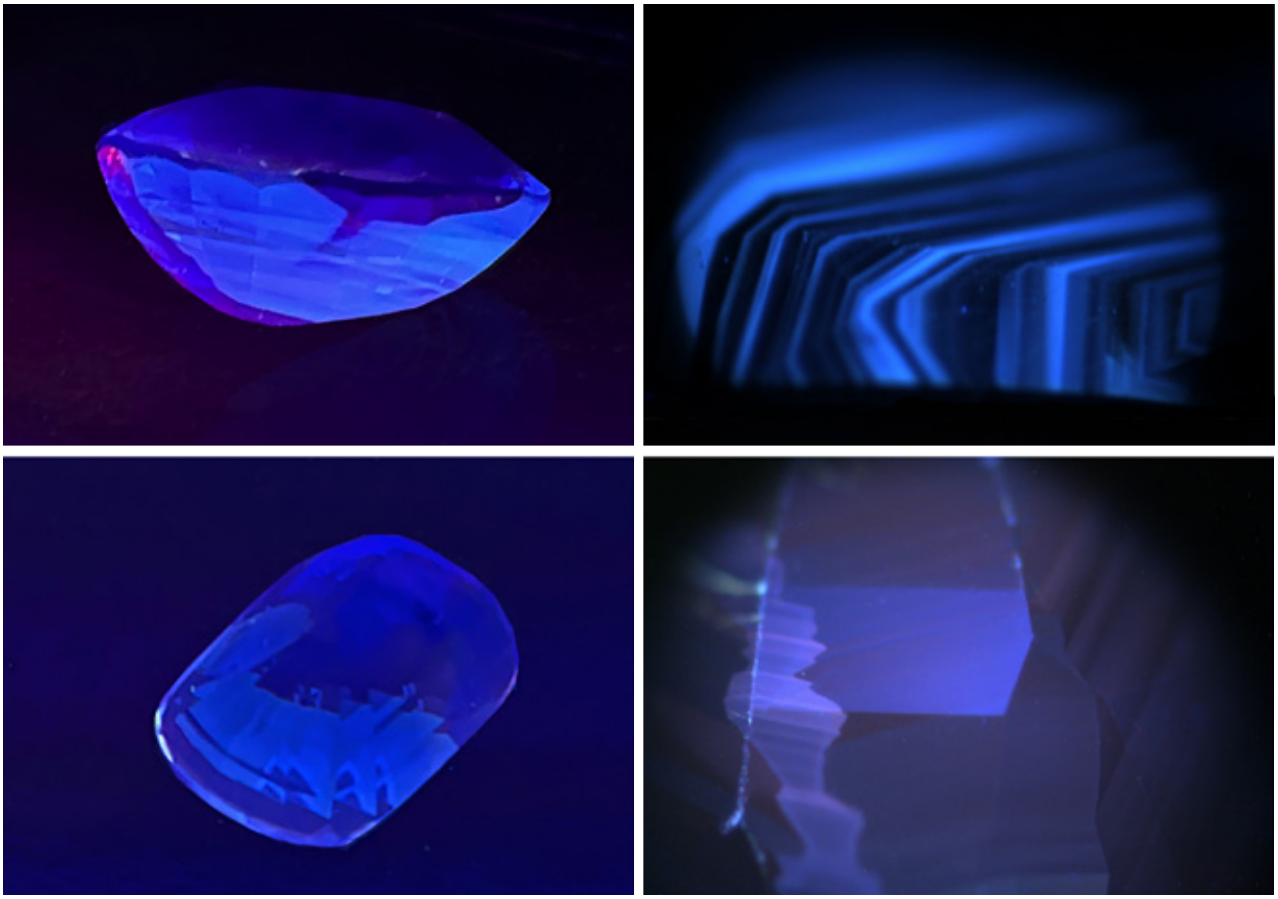

Figure 12: These examples of zoned 'chalky' bluish white reactions represent the typical response of all the investigated unheated HFSE-enriched sapphires when exposed to a short-wave UV lamp or the ultra-short-wave UV source of a DiamondView instrument. Photos by M. S. Krzemnicki and J. Braun; magnified 5× (left side) and 30× (right side).

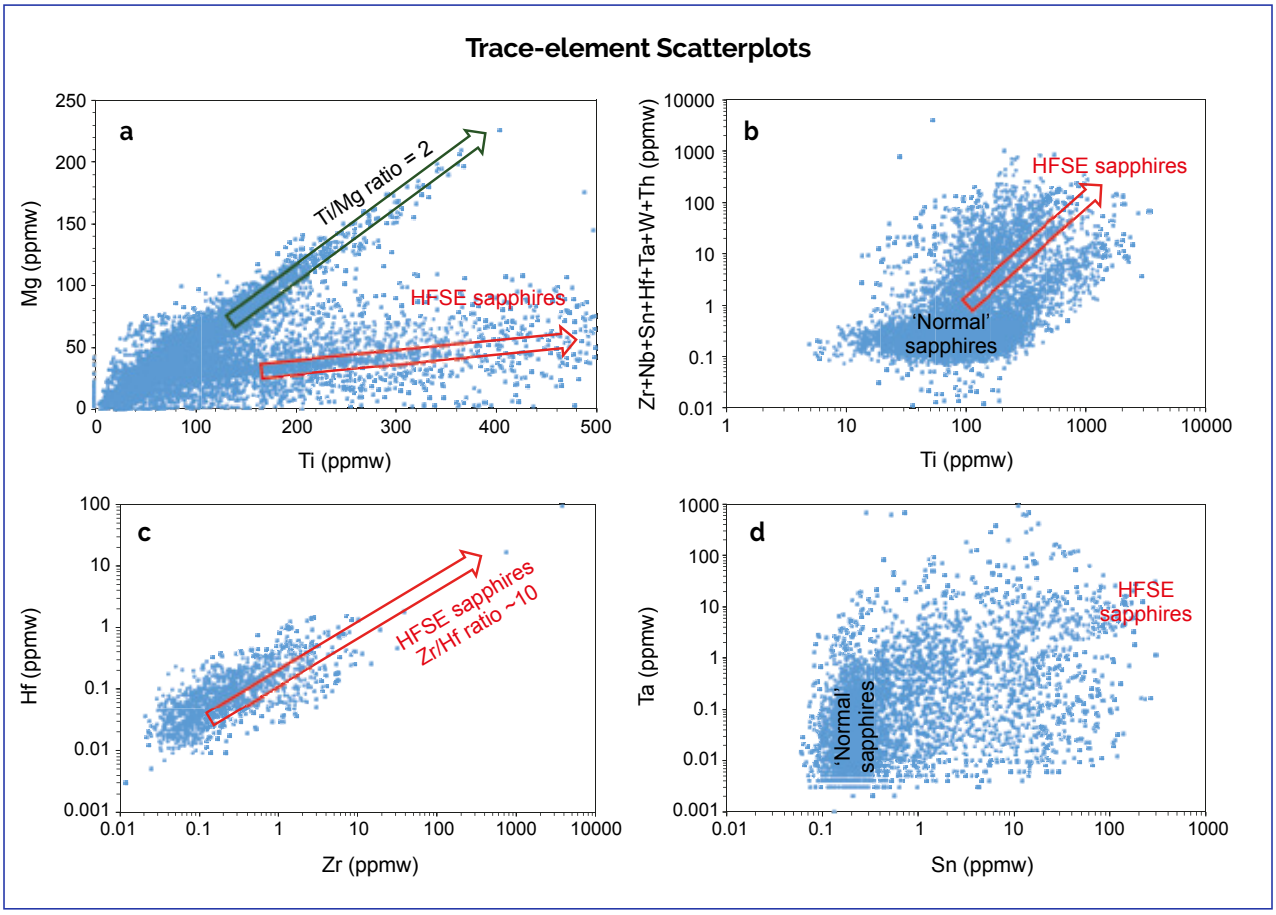

Figure 13: Various trace-element scatterplots are shown for metamorphic blue sapphires analysed by GemTOF in the past 10 years at SSEF. (**a**) A plot of Ti vs Mg reveals different trends for the Ti/Mg ratio in HFSE-enriched sapphires compared to 'normal' sapphires. Plots of (**b**) Ti vs the HFSE sum and (**c**) Zr vs Hf both show positive correlation trends. (**d**) A plot of Sn vs Ta reveals generally lower contents of both elements in 'normal' sapphires, but otherwise no systematic correlation between these elements.

The chemical data for the 24 HFSE-enriched sapphires investigated in this study further refined these general trends. Table I illustrates the pronounced variability in HFSE concentrations compared to a representative HFSE-poor Burmese sapphire.[1] As expected from previous studies (Jin *et al*. 2024 and references therein), HFSE-enriched sapphires may also contain measurable Be and B, elements typically below the detection limits in untreated metamorphic corundum (Dubinsky *et al*. 2020). Consistently, their Ti/Mg ratios were significantly elevated (mostly Ti/Mg ≥ 5) compared to the reference Burmese sapphire sample (Ti/Mg = 2.0).

In general, as shown in Table II, the HFSE-enriched sapphires analysed for this report exhibited either (1) strong intra-stone chemical variability, with HFSE concentrations varying by several orders of magnitude within a single sample (e.g. Ta ranging from 0.07 to 346 ppmw), or (2) relatively homogeneous composition (e.g. Ta consistently 138–142 ppmw). Sample S_439 (Figure 14) illustrates the chemically heterogeneous type particularly well. Although it displayed visually homogeneous blue colouration face-up, it showed clear internal zoning with the microscope. A narrow colourless band crossing the girdle and pavilion corresponded to a region of much stronger short-wave UV fluorescence, highlighting chemical zoning within the stone. Of the five GemTOF spots analysed along the stone's girdle (Table III), only spot no. 2 coincided with this narrow colourless fluorescent

[1] It should be noted that the mean analyses in Table I are somewhat misleading, as these data do not capture the pronounced chemical heterogeneity commonly present in unheated HFSE-enriched sapphires (as also reflected in their distinct colour zoning; Figure 6). This limitation is further affected by the analytical approach, as only a small number of laser-ablation spots (typically four per sample) were measured, usually positioned arbitrarily along the girdle. As a result, the obtained trace-element data may not represent the full internal chemical variability of a particular sapphire.

Table I: Mean trace-element data (by GemTOF; in ppmw) of seven of the HFSE-enriched sapphires investigated for this study, compared with a 'normal' (HFSE-poor) sapphire from Myanmar.*

Sample type	HFSE-enriched sapphires							Burmese sapphire	Detection limit
Sample no.	S_264	S_032	S_492	S_721	S_439	S_570	S_610	SH_696	
Stone image									
No. analyses	4	4	4	4	5	4	4	4	
Be	1.79	0.74	0.85	3.08	2.19	2.56	bdl	bdl	0.36
B	3.57	6.27	3.05	3.14	2.16	1.45	0.76	0.16	0.35
Mg	43.9	36.1	35.9	12.5	47.2	52.8	63.3	38.7	0.04
Ti	527	83.2	560	116	237	296	1310	78.6	0.28
V	13.8	5.93	12.4	3.05	15.0	14.8	16.1	8.23	0.02
Cr	0.41	0.93	0.65	0.43	0.66	2.28	2.35	1.21	0.14
Fe	413	395	631	417	761	707	410	1160	0.51
Ga	76.4	15.0	72.1	56.9	69.3	63.8	72.7	93.2	0.01
Zr	0.68	0.05	0.14	0.03	0.37	0.40	0.63	bdl	0.02
Nb	4.91	2.47	1.27	3.68	10.8	9.00	0.40	bdl	0.01
Sn	78.8	22.1	24.0	440	28.5	29.2	54.0	0.14	0.02
Hf	0.33	0.01	0.07	0.04	0.14	0.17	0.08	bdl	0.01
Ta	44.0	66.8	10.4	12.6	97.8	65.7	0.24	bdl	0.01
W	3.00	1.93	0.35	0.07	13.1	9.65	0.10	bdl	0.01
Th	0.40	bdl	2.31	bdl	0.04	0.02	0.13	bdl	0.01
HFSE sum	132	93.4	38.5	456	151	114	55.6	0.14	na
Ti/Mg	12.0	2.3	15.6	9.3	5.0	5.6	20.7	2.0	na

* Blue shading indicates HFSE. Abbreviations: bdl = below detection limit; na = not applicable. Photos by L. Phan, SSEF.

zone. This spot showed pronounced HFSE enrichment, including 481 ppmw Ta and a total HFSE concentration of 622 ppmw, accompanied by elevated Be and B. By contrast, the remaining four spots, located in the blue areas of the sapphire, showed substantially lower HFSE concentrations (except for Sn), although still higher than those observed in typical HFSE-poor sapphires such as the Burmese reference sample (again, see Table I).

FTIR Spectroscopy

The internal chemical variability and zoning in the HFSE-enriched sapphires mentioned above likely contribute to the diversity of their FTIR spectra, as seen in Figure 15. (See Table DD-2 for trace-element analyses of all the samples represented in Figure 15.)

Many of the investigated HFSE-enriched sapphires displayed a broad absorption band near 3300 cm^{-1} in their FTIR spectra (Figure 15a). This feature in the OH-stretching region of corundum (Beran & Rossman 2006) varied in intensity from weak to, in some cases, dominant. Although no clear correlation has been observed between its intensity and specific trace elements (e.g. Ti or HFSE, including Sn), according to SSEF's database all sapphires exhibiting this band have been found to be HFSE-enriched. Visually, these stones typically show fine growth zoning with distinct 'inky' blue colour bands (e.g. Figure 6) and generally only weak turbidity.

In the sample subset shown in Figure 15b, the 3300 cm^{-1} band was weak or nearly absent, and was instead overprinted by a triplet of sharp peaks at 3309, 3232 and 3185 cm^{-1}, commonly referred to as the '3309 cm^{-1} series'. This feature has been attributed to Ti^{4+}–OH^{-} complexes associated with aluminium vacancies (Moon & Phillips 1991; Beran & Rossman 2006; Jollands *et al*. 2023 and references therein). Trace-element data indicated no significant compositional differences between sapphires showing the broad 3300 cm^{-1} band and those dominated by the 3309 cm^{-1} series.

In some cases (i.e. the samples in Figure 15c), the

Table II: Trace-element data (by GemTOF; in ppmw) for representative sapphires showing strong chemical inhomogeneity and a more homogeneous composition.*

Composition	Inhomogeneous		Homogeneous	
Sample no.	S_973		S_252	
Stone image				
Value	Minimum	Maximum	Minimum	Maximum
Be	bdl	11.2	2.27	4.73
B	bdl	4.39	5.32	6.78
Mg	23.4	62.1	47.1	49.6
Ti	187	261	111	117
V	12.3	19.9	14.0	14.2
Cr	1.09	1.69	1.53	2.57
Fe	566	846	723	770
Ga	69.5	84.0	95.4	99.3
Zr	bdl	0.71	0.18	0.23
Nb	bdl	34.7	14.5	15.0
Sn	0.81	38.6	8.97	9.56
Hf	bdl	0.14	0.03	0.05
Ta	0.07	346	138	142
W	bdl	42.7	13.7	15.0
Th	bdl	0.04	bdl	bdl
HFSE sum	1.59	440	175	182
Ti/Mg	8.0	4.2	2.3	2.4

* Blue shading indicates HFSE. Abbreviation: bdl = below detection limit. Photos by L. Phan, SSEF.

Table III: Trace-element data (by GemTOF; in ppmw) of five spots measured on the girdle of sapphire S_439 (see Figure 14).*

Spot no.	1	2	3	4	5
Be	bdl	11.0	bdl	bdl	bdl
B	1.66	5.92	1.31	0.73	1.16
Mg	52.5	60.9	45.1	38.6	38.8
Ti	316	285	229	187	167
V	16.2	19.6	14.1	13.2	12.1
Cr	0.98	0.84	0.58	0.53	0.38
Fe	853	692	768	761	730
Ga	72.4	68.3	69.4	68.8	67.6
Zr	0.28	**1.24**	0.13	0.12	0.07
Nb	0.07	**53.4**	0.29	0.01	bdl
Sn	44.1	21.2	30.0	29.0	18.3
Hf	0.17	**0.24**	0.10	0.10	0.07
Ta	2.76	**481**	3.03	1.73	0.96
W	bdl	**65.0**	0.27	bdl	bdl
Th	bdl	**0.22**	bdl	bdl	bdl
HFSE sum	47.4	**622**	33.8	31.0	19.4
Ti/Mg	6.0	4.7	5.1	4.8	4.3

* Spot no. 2 analysed a colourless zone with chalky bluish white short-wave UV fluorescence. Blue shading indicates HFSE, with bold font indicating the enrichment in HFSE (except for Sn) in the colourless zone. Abbreviation: bdl = below detection limit.

3309 cm^{-1} triplet became dominant, while the broad 3300 cm^{-1} band was absent or only very weak. In this subset, the HFSE-enriched sapphires typically appeared relatively homogeneous, with moderate turbidity, fine growth zoning and few additional inclusions. This behaviour also correlated with more uniform trace-element distributions and comparatively moderate to rather low total HFSE contents (approximately 10–25 ppmw).

A small number of samples (Figure 15d) exhibited a distinct 3162 cm^{-1} peak, accompanied by bands

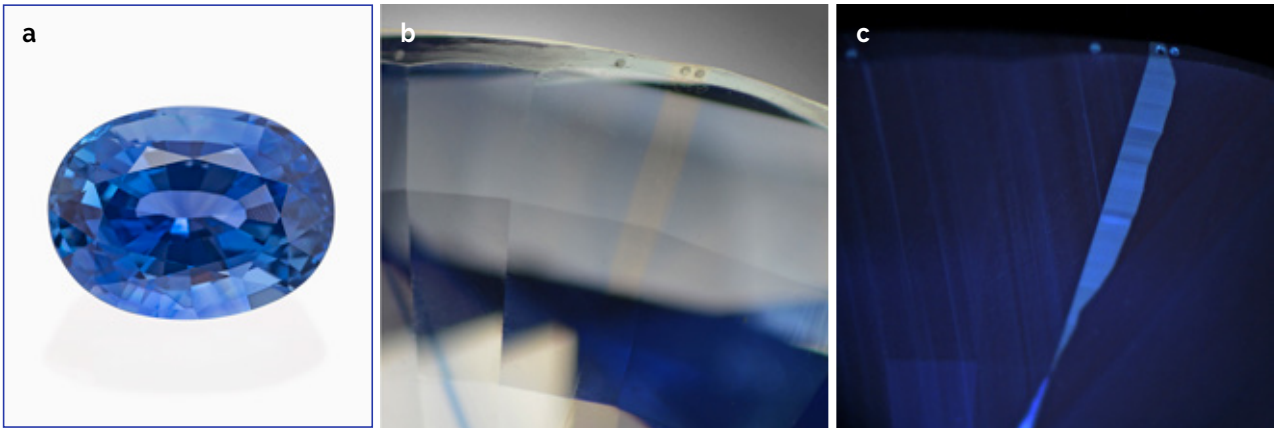

Figure 14: (**a**) Unheated sapphire S_439 (5.48 ct) contains a narrow zone enriched in HFSE that is visible (**b**) with a microscope as a colourless band and (**c**) in the DiamondView as a chalky bluish white zone. The positions of the analytical spots seen on the girdle show that only one captured the distinct chemical composition of this zone (see Table III). Photo by (a) L. Phan, SSEF, and photomicrographs by (b) M. S. Krzemnicki and (c) M. Wälle, both magnified 50×.

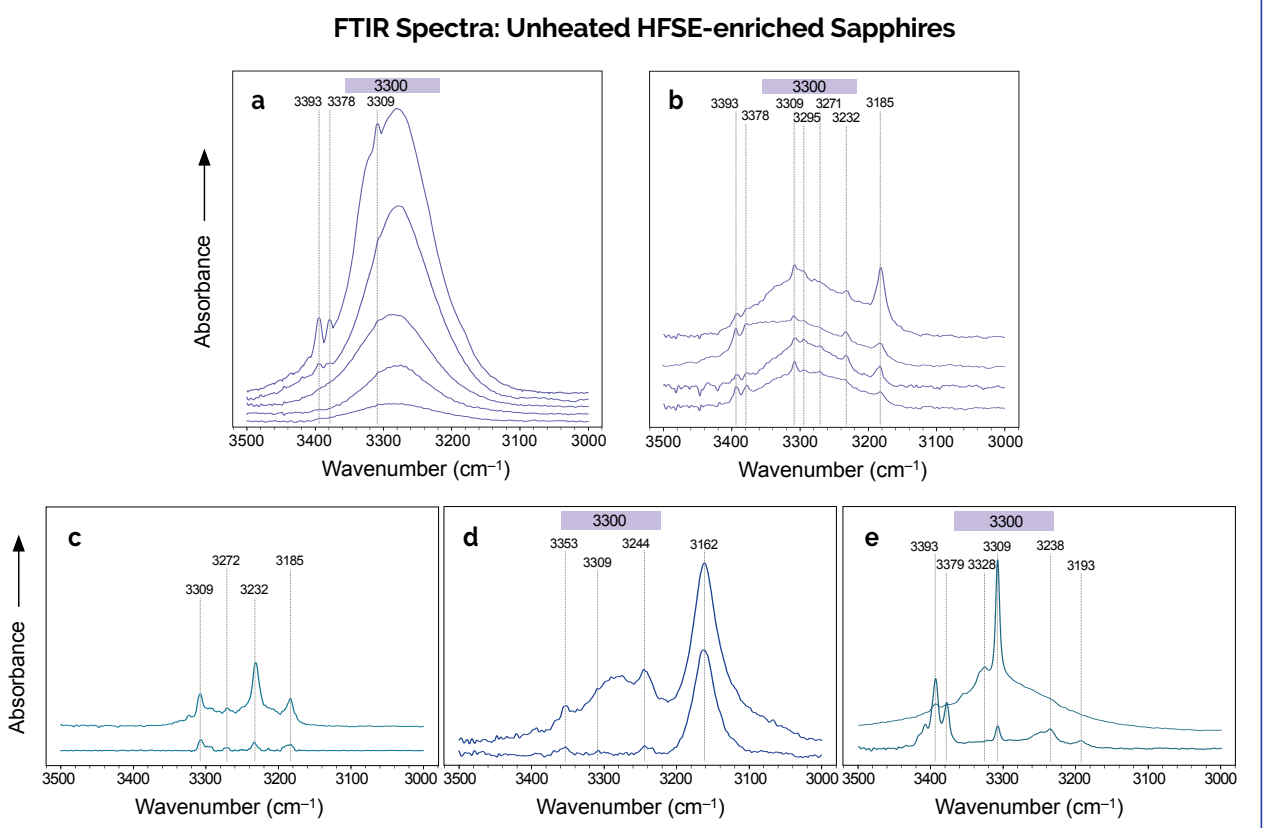

Figure 15: FTIR spectra of the HFSE-enriched sapphires investigated for this study (see Table DD-2) fell into five groups of, mostly, similar features. (**a**) Many samples showed a weak-to-strong broad absorption band at about 3300 cm^{-1} in the OH-stretching region. (**b**) Another group showed a relatively weak 3300 cm^{-1} absorption band accompanied by the triplet peaks of the 3309 cm^{-1} series. Although the 3309 cm^{-1} series has been used as an indication of heat treatment, none of these HFSE-enriched sapphires had been heated. (**c**) Some of the samples revealed a dominant 3309 cm^{-1} triplet with no or only a very weak 3300 cm^{-1} absorption band. (**d**) A small number of the sapphires showed a 3162 cm^{-1} peak (and its series, including peaks at 3353 and 3244 cm^{-1}), with or without the 3300 cm^{-1} band. (**e**) Two samples yielded atypical FTIR spectra. These included (upper spectrum) a strong 3309 cm^{-1} peak and 3328 cm^{-1} shoulder, and (lower spectrum) a series of bands attributed to Sn (Jollands *et al.* 2025). The spectra are offset vertically for clarity.

at 3353 and 3244 cm^{-1} (the '3160 cm^{-1} series'), which has been commonly associated with Mg^{2+}–OH^- complexes in Fe-poor corundum (Balmer *et al.* 2006; Smith & van der Bogert 2006). The 3160 cm^{-1} series is well known in unheated metamorphic yellow sapphires (e.g. from Sri Lanka and Madagascar) and is considered a useful indicator of unheated material, as it progressively disappears at temperatures of approximately 700–900°C (Atikarnsakul & Emmett 2021). In this study, this spectral type appeared only in HFSE-enriched sapphires with low and homogeneous Ti/Mg ratios of about 2.

Two samples displayed atypical FTIR spectra. The upper spectrum in Figure 15e shows a very strong 3309 cm^{-1} peak with a shoulder at 3328 cm^{-1}, superimposed on a broad band resembling the 3300 cm^{-1} feature in Figure 15a. The lower spectrum exhibits a more complex pattern of peaks, which have been attributed to Sn-related defects (Jollands *et al.* 2025; cf. figure 1, spectrum I, in that article). Notably, this spectral type was an isolated case in our study, and no comparable spectra were observed in any of the other samples, including those with a very high Sn concentration (>100 ppmw).

Relevance for the Detection of Heat Treatment in Sapphires

In the past decade, the authors have investigated a large number of HFSE-enriched sapphires (Figure 3), predominantly of metamorphic origin (mainly from Sri Lanka and Madagascar). As demonstrated by the 24 unheated samples presented in this study, these sapphires commonly show diagnostic microscopic features, including fine growth zoning, pronounced colour banding, and turbidity caused by sub-microscopic inclusions. This internal zoning is also reflected in their chemical composition, which is often highly heterogeneous, particularly with respect to HFSE (e.g. Zr, Nb, Sn, Hf, Ta, W and Th). Consequently, the FTIR spectra of these sapphires show considerable variability.

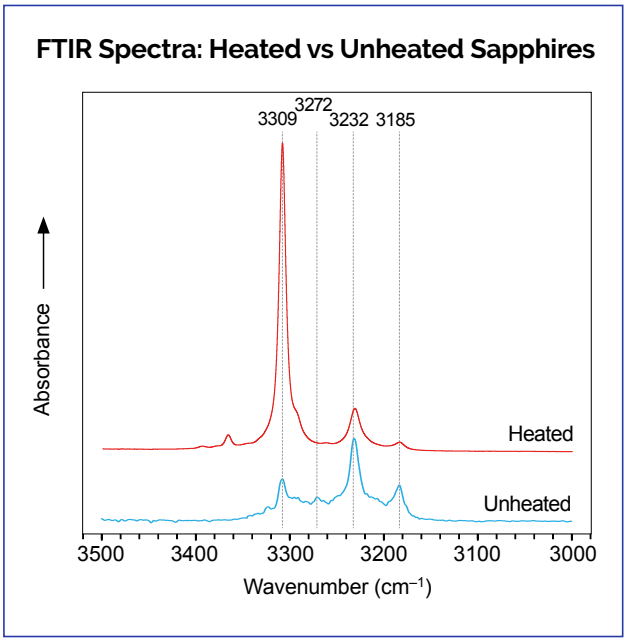

Figure 16: A comparison of the FTIR spectra of unheated and heated sapphires, both similarly enriched in HFSE, reveals a significantly stronger 3309 cm^{-1} peak after heating, dominating the other two peaks in the series. The large variations seen in the spectra of HFSE-enriched sapphires (see Figure 15), however, suggest that this alone may not be a reliable indicator of heat treatment. The spectra have been offset vertically for clarity.

A recurring feature is a broad absorption band around 3300 cm^{-1} (Figure 15a). In our experience, sapphires exhibiting this band—regardless of its intensity—consistently show elevated HFSE contents compared to typical metamorphic sapphires, which are generally HFSE-poor except for traces of Sn (<1 ppmw).

Interestingly, some unheated HFSE-enriched sapphires also display the 3309, 3232 and 3185 cm^{-1} triplet (or '3309 cm^{-1} series'; see Figure 15b, c), a feature (specifically the 3232 cm^{-1} peak) that is often used as an indicator of heat treatment (Smith 1995; Krzemnicki 2019; Saeseaw *et al*. 2020; Curti *et al*. 2025; Delaunay *et al*. 2026). However, in contrast to heat-treated or naturally heated basaltic sapphires—where the 3309 cm^{-1} peak strongly dominates (Soonthorntantikul & Palke 2025) and the baseline is typically flat—unheated HFSE-enriched samples show a more balanced triplet, with the 3309 cm^{-1} peak often comparable to or even weaker than the 3232 and 3185 cm^{-1} peaks (Figure 15c), and frequently a residual broad 3300 cm^{-1} absorption is retained (Figure 15b).

Figure 16 illustrates this difference using two HFSE-enriched sapphires with similar total HFSE contents (about 15–20 ppmw). (Again, see Table DD-2 for trace-element analyses of the samples represented in this figure.) Based on additional heated metamorphic HFSE samples from SSEF's database, we infer that high-temperature treatment (presumably >1,200°C) not only converts Ti^{4+}–OH^{-}-related defects into producing the dominant 3309 cm^{-1} feature but it also suppresses the underlying broad 3300 cm^{-1} band. This empirical observation is based on 25 heated metamorphic HFSE sapphires examined at SSEF that all show strong 'classic' 3309 cm^{-1}-series peaks but no broad band at 3300 cm^{-1}.

Most of the unheated HFSE-enriched sapphires also exhibited a chalky bluish white response under short-wave UV radiation, often showing zonation (Figures 12, 14c and 17, left). This behaviour is also well known in heat-treated metamorphic sapphires (Hughes & Emmett 2005; Hughes & Perkins 2019; see also Figure 17, right). Accordingly, short-wave UV fluorescence alone cannot be considered a reliable indicator of heat treatment without knowing the trace-element composition of the sapphire.

CONCLUSIONS

This study of 24 selected unheated metamorphic sapphires enriched in HFSE (e.g. Zr, Nb, Sn, Hf, Ta, W and Th) highlights their strong variability in trace-element composition, FTIR spectroscopic characteristics and short-wave UV fluorescence behaviour. These sapphires formed under metamorphic conditions influenced by localised fluid activity (metasomatism) and have come from several deposits worldwide, most notably in Sri Lanka and Madagascar. Many of these stones reach considerable size and are of high gem quality. They commonly display pronounced growth

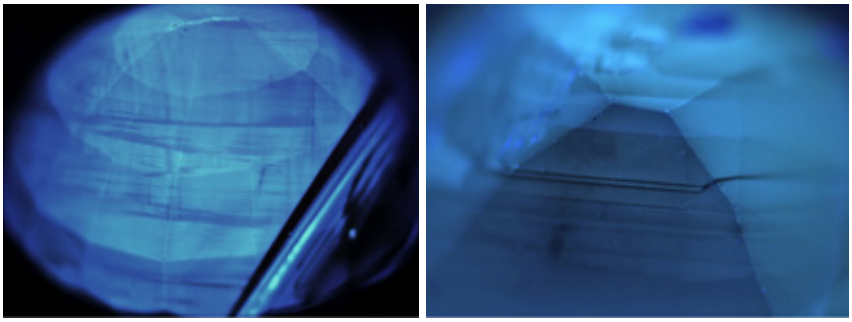

Figure 17: An unheated metamorphic HFSE-enriched sapphire (left) and a heated metamorphic sapphire (right) exhibit similar chalky bluish white luminescence to the ultra-short-wave UV radiation of the DiamondView. Photomicrographs by M. Wälle; magnified 30×.

zoning and turbidity caused by sub-microscopic inclusions, the latter of which produces an attractive velvety blue appearance.

The aim of this study was to assess the influence of elevated HFSE concentrations on sapphire properties, particularly their FTIR spectra and short-wave UV fluorescence. The results show that HFSE enrichment complicates some criteria traditionally used for heat-treatment detection in corundum. In particular, neither the presence of the 3309 cm^{-1} triplet (including the 3232 cm^{-1} peak) nor chalky short-wave UV fluorescence can be considered definitive indicators of heat treatment in sapphire.

This is consistent with recent observations of unheated pink sapphires from Ilakaka (Madagascar) exhibiting the same 3309 cm^{-1} triplet (Gao *et al*. 2025; Krzemnicki *et al*. 2025a). Accordingly, reliable discrimination between heated and unheated metamorphic sapphires requires a combined approach, integrating detailed microscopic examination of inclusions with advanced analytical techniques (e.g. LA-ICP-MS or GemTOF) for trace-element characterisation, and Raman micro-spectroscopy of diagnostic inclusions (e.g. goethite and diaspore).

REFERENCES

Allirol-Mouton, C., Notari, F. & Blumentritt, F. 2025. Un remarquable saphir "ottu" au laboratoire. *Gemmes*, No. 6, 10–21, https://doi.org/10.63000/G6camV225y8E4a.

Atikarnsakul, U. & Emmett, J.L. 2021. Gem News International: Heat treatment effects on the behavior of the 3161 cm^{-1} feature in low-iron metamorphic yellow sapphire. *Gems & Gemology*, **57**(3), 286–288.

Balmer, W.A., Leelawatanasuk, T., Atichat, W., Wathanakul, P. & Somboon, C. 2006. Update on FTIR characteristics of heated and unheated yellow sapphires. *1st GIT International Gem & Jewelry Conference (GIT 2006)*, Bangkok, Thailand, 5–9 December, 91.

Beran, A. & Rossman, G.R. 2006. OH in naturally occurring corundum. *European Journal of Mineralogy*, **18**(4), 441–447, https://doi.org/10.1127/0935-1221/2006/0018-0441.

Choudhary, G. 2006. Gem News International: Sapphire with unusual color zoning. *Gems & Gemology*, **42**(1), 74–75.

Curti, M., Ellia, H., Musilli, G., Rozet, T., Fejoz, V., Guzzi, C., Hinnemann, P. & Marlin, E. 2025. Ilakaka's pink sapphire conundrum: Statistical analysis of ν^3 antisymmetric stretching in zircon (SiO_4) as a thermal history indicator. *InColor*, No. 53, 42–56.

Delaunay, A., Hennebois, U., Fritsch, E. & Karampelas, S. 2026. Gem Notes: A metamorphic-type sapphire containing diaspore inclusions and the '3309 cm^{-1} series' FTIR bands. *Journal of Gemmology*, **40**(1), 10–12, https://doi.org/10.15506/JoG.2026.40.1.10.

Dubinsky, E.V., Stone-Sundberg, J. & Emmett, J.L. 2020. A quantitative description of the causes of color in corundum. *Gems & Gemology*, **56**(1), 2–28, https://doi.org/10.5741/gems.56.1.2.

Dutrow, B.L., Henry, D.J. & Sun, Z. 2019. Origin of corundum–tourmaline–phlogopite rocks from Badakhshan, northeastern Afghanistan: A new type of metasomatism associated with sapphire formation. *European Journal of Mineralogy*, **31**(4), 739–753, https://doi.org/10.1127/ejm/2019/0031-2881.

Emori, K., Oto, S., Igami, Y., Uzuhashi, J., Ohkubo, T., Kitawaki, H. & Miyake, A. 2024. Nano-inclusions associated with beryllium in untreated blue sapphires from Diego Suarez, Madagascar. *Journal of Gemmology*, **39**(4), 364–372, https://doi.org/10.15506/jog.2024.39.4.364.

Gao, Y., Huang, T. & Lucas, A. 2025. Gem Notes: A pink sapphire with questionable heat treatment. *Journal of Gemmology*, **39**(8), 736–738, https://doi.org/10.15506/JoG.2025.39.8.736.

Gialanella, S., Girardi, F., Ischia, G., Lonardelli, I., Mattarelli, M. & Montagna, M. 2010. On the goethite to hematite phase transformation. *Journal of Thermal Analysis and Calorimetry*, **102**(3), 867–873, https://doi.org/10.1007/s10973-010-0756-2.

Giuliani, G., Ohnenstetter, D., Fallick, A.E., Groat, L. & Fagan, A.J. 2014. The geology and genesis of gem corundum deposits. *In*: Groat, L.A. (ed) *Geology of Gem Deposits*, 2nd edn. Mineralogical Association of Canada Short Course Series 44, 29–112, https://doi.org/10.3749/9780921294696.ch02.

Gübelin, E.J. & Peretti, A. 1997. Sapphires from the Andranondambo mine in SE Madagascar: Evidence for metasomatic skarn formation. *Journal of Gemmology*, **25**(7), 453–470, https://doi.org/10.15506/JoG.1997.25.7.453.

Hänni, H.A. 1994. Origin determination for gemstones: Possibilities, restrictions and reliability. *Journal of Gemmology*, **24**(3), 139–148, https://doi.org/10.15506/JoG.1994.24.3.139.

Hughes, R.W. & Emmett, J.L. 2005. Heat seeker—UV fluorescence as a gemological tool. Lotus Gemology, https://lotusgemology.com/resources/articles/156-heat-seeker-uv-fluorescence-as-a-gemological-tool, accessed 2 May 2026.

Hughes, E.B. & Perkins, R. 2019. Madagascar sapphire: Low-temperature heat treatment experiments. *Gems & Gemology*, **55**(2), 184–197, https://doi.org/10.5741/gems.55.2.184.

Jaireth, S., Hoatson, D.M. & Miezitis, Y. 2014. Geological setting and resources of the major rare-earth-element deposits in Australia. *Ore Geology Reviews*, **62**, 72–128, https://doi.org/10.1016/j.oregeorev.2014.02.008.

Jiang, S.Y., Wang, R.C., Xu, X.S. & Zhao, K.D. 2005. Mobility of high field strength elements (HFSE) in magmatic-, metamorphic-, and submarine-hydrothermal

systems. *Physics and Chemistry of the Earth, Parts A/B/C*, **30**(17–18), 1020–1029, https://doi.org/10.1016/j.pce.2004.11.004.

Jin, S., Saxey, D.W., Quadir, Z., Reddy, S.M., Rickard, W.D.A., Fougerouse, D., Sun, X. & Palke, A.C. 2024. Nanoparticles in natural beryllium-bearing sapphire: Incorporation and exsolution of high field strength elements in corundum. *Contributions to Mineralogy and Petrology*, **179**(12), article 110, https://doi.org/10.1007/s00410-024-02189-y.

Jollands, M.C., Jin, S., Curti, M., Guillaumet, M., Béneut, K., Giura, P. & Balan, E. 2023. Vibrational properties of OH groups associated with divalent cations in corundum (α-Al_2O_3). *European Journal of Mineralogy*, **35**(5), 873–890, https://doi.org/10.5194/ejm-35-873-2023.

Jollands, M.C., Bishop, K., Smith, T., Jin, S. & Balan, E. 2025. Defects associated with Sn (±Ti) and H in corundum (Al_2O_3). *Materialia*, **41**, article 102434, https://doi.org/10.1016/j.mtla.2025.102434.

Kammerling, R.C. & Koivula, J.I. 1989. Thermal alteration of inclusions in "rutilated" topaz. *Gems & Gemology*, **25**(3), 165–167.

Karampelas, S., Hennebois, U., Mevellec, J.-Y., Pardieu, V., Delaunay, A. & Fritsch, E. 2023. Pink to purple sapphires from Ilakaka, Madagascar: Insights to separate unheated from heated samples. *Minerals*, **13**(5), article 704, https://doi.org/10.3390/min13050704.

Koivula, J.I. 1987. Goethite inclusion alteration during the heat conversion of amethyst to citrine. *Australian Gemmologist*, **16**, 271–272.

Koivula, J.I. 2013. Useful visual clue indicating corundum heat treatment. *Gems & Gemology*, **49**(3), 160–161, https://doi.org/10.5741/gems.49.3.160.

Krzemnicki, M.S. 2019. Detection of low-temperature heated rubies from Mozambique. *Facette Magazine*, No. 25, 9, https://tinyurl.com/2bxwz26k.

Krzemnicki, M.S., Pettke, T. & Hänni, H.A. 2007. Laser ablation inductively coupled plasma mass spectrometry (LA-ICP-MS), a new method for gemstone analysis. *Journal of the Gemmological Association of Hong Kong*, **28**, 31–35.

Krzemnicki, M.S., Wang, H.A.O. & Phyo, M.M. 2019. Age dating applied as a testing procedure to gemstones and biogenic gem materials. *36th International Gemmological Conference*, Nantes, France, 28–31 August, 48–50, https://tinyurl.com/mt22x26w.

Krzemnicki, M.S., Lefèvre, P., Zhou, W., Braun, J. & Spiekermann, G. 2023. Dehydration of diaspore and goethite during low-temperature heating as criterion to separate unheated from heated rubies and sapphires. *Minerals*, **13**(12), article 1557, https://doi.org/10.3390/min13121557.

Krzemnicki, M.S., Wang, H.A.O., Sun, Y., Beney, I. & Wälle, M. 2025a. Gem Notes: Unheated pink sapphire from Madagascar with OH-related 3232 and 3185 cm^{-1} FTIR bands. *Journal of Gemmology*, **39**(8), 734–736, https://doi.org/10.15506/JoG.2025.39.8.734.

Krzemnicki, M.S., Zhou, W., Lefèvre, P., Wälle, M. & Wang, H. 2025b. HFSE-enriched sapphires of gem quality: A combined FTIR and trace element study and implications for heat treatment detection. *38th International Gemmological Conference*, Athens, Greece, 20–24 October, 122–124, https://tinyurl.com/2t8yyr6c.

McGee, B.M. 2005. *Characteristics and origin of the Weldborough sapphire, NE Tasmania.* BSc thesis, University of Tasmania, Australia, 118 pp., https://tinyurl.com/4nnfx99b.

Miranda-Díaz, G., Riveros-Jensen, K., Heide, G., Menzies, A., Griem, W., Araya-Tabilo, E., Añasco-Leyton, G. & Medina, E. 2022. Geology and mineralogy of sapphire-rich metasomatites (sapphirites) deposit at the Portezuelo de Pajas Blancas, northern Chile: Genetic implications for unusual metasomatic processes in the Central Andes. *Ore Geology Reviews*, **141**, article 104646, https://doi.org/10.1016/j.oregeorev.2021.104646.

Moon, A.R. & Phillips, M.R. 1991. Titania precipitation in sapphire containing iron and titanium. *Physics and Chemistry of Minerals*, **18**(4), 251–258, https://doi.org/10.1007/bf00202577.

Nasdala, L., Irmer, G. & Wolf, D. 1995. The degree of metamictization in zircon: A Raman spectroscopic study. *European Journal of Mineralogy*, **7**(3), 471–478, https://doi.org/10.1127/ejm/7/3/0471.

Oto, S., Miyake, A., Igami, Y., Emori, K. & Kitawaki, H. 2023. Crystal structure of nano inclusions in blue sapphire from Diego Suarez, northern Madagascar. *37th International Gemmological Conference*, Tokyo, Japan, 23–27 October, 135–137, https://tinyurl.com/5628d5jc.

Pannipitiye, G.R., Dharmaratne, H.M., Premasiri, R. & Dillimuni, D. 2012. Sapphires from Thammannawa, Kataragama area, Sri Lanka. *Gems & Gemology*, **48**(2), 98–107, https://doi.org/10.5741/GEMS.48.2.98.

Pardieu, V. 2007. Beryllium discovered in unheated sapphires. *InColor*, No. 6, 41.

Pardieu, V. 2013. Blue sapphires and beryllium: 'An unfinished world quest'. *InColor*, No. 23, 36–43.

Pardieu, V. & Klemm, L. 2008. Nouvelles des travaux sur le béryllium et les saphirs bleus. *Revue de Gemmologie A.F.G.*, No. 163, 7–9.

Pardieu, V., Saeseaw, S., Thirangoon, K. & Lomthong, P. 2011. Lab Notes: Beryllium- and tungsten-bearing sapphires from Afghanistan. *Gems & Gemology*, **47**(1), 53–54.

Rollinson, H.R. 1993. *Using Geochemical Data: Evaluation, Presentation, Interpretation*. Longman Scientific & Technical, Harlow, Essex, 352 pp.

Saeseaw, S., Sangsawong, S., Vertriest, W. & Atikarnsakul, U. 2017. GIA News from Research: An In-depth Study of Blue Sapphires from Pailin, Cambodia. Gemological Institute of America, 45 pp.

Saeseaw, S., Khowpong, C. & Vertriest, W. 2020. Low-temperature heat treatment of pink sapphires from Ilakaka, Madagascar. *Gems & Gemology*, **56**(4), 448–457, https://doi.org/10.5741/gems.56.4.448.

Salters, V. 2016. High field strength elements. *In*: White, W.M. (ed) *Encyclopedia of Geochemistry*. Springer, Cham, Switzerland, 3 pp., https://doi.org/10.1007/978-3-319-39193-9_278-1.

Schwarz, D., Petsch, E.J. & Kanis, J. 1996. Sapphires from the Andranondambo region, Madagascar. *Gems & Gemology*, **32**(2), 80–99, https://doi.org/10.5741/gems.32.2.80.

Shen, A., McClure, S., Breeding, C.M., Scarratt, K., Wang, W., Smith, C. & Shigley, J. 2007. From the GIA Laboratory: Beryllium in corundum – The consequences for blue sapphire. *GIA Insider*, **9**(2), 26 January.

Shen, A.H. 2011. The nature of the Be-Nb-Ta containing cloud in natural Madagascar blue sapphire – An FIB/HRTEM study. Gemological Institute of America, 15 pp.

Shen, A.H. & Wirth, R. 2012. Gem News International: Beryllium-bearing nano-inclusions identified in untreated Madagascar sapphire. *Gems & Gemology*, **48**(2), 150–151.

Simonet, C., Fritsch, E. & Lasnier, B. 2008. A classification of gem corundum deposits aimed towards gem exploration. *Ore Geology Reviews*, **34**(1–2), 127–133, https://doi.org/10.1016/j.oregeorev.2007.09.002.

Smith, C.P. 1995. A contribution to understanding the infrared spectra of rubies from Mong Hsu, Myanmar. *Journal of Gemmology*, **24**(5), 321–335, https://doi.org/10.15506/JoG.1995.24.5.321.

Smith, C.P. & van der Bogert, C. 2006. Infrared spectra of gem corundum. *Gems & Gemology*, **42**(3), 92–93.

Soonthorntantikul, W. & Palke, A.C. 2025. The 3309 cm^{-1} series in sapphire and ruby: A focus on FTIR peak position variation. *Gems & Gemology*, **61**(1), 2–15, https://doi.org/10.5741/gems.61.1.2.

Sripoonjan, T., Wanthanachaisaeng, B. & Leelawatanasuk, T. 2016. Phase transformation of epigenetic iron staining: Indication of low-temperature heat treatment in Mozambique ruby. *Journal of Gemmology*, **35**(2), 156–161, https://doi.org/10.15506/JoG.2016.35.2.156.

Upton, B.G.J., Hinton, R.W., Aspen, P., Finch, A. & Valley, J.W. 1999. Megacrysts and associated xenoliths: Evidence for migration of geochemically enriched melts in the upper mantle beneath Scotland. *Journal of Petrology*, **40**(6), 935–956, https://doi.org/10.1093/petroj/40.6.935.

Vigier, M., Fritsch, E., Cavignac, T., Latouche, C. & Jobic, S. 2023. Shortwave UV blue luminescence of some minerals and gems due to titanate groups. *Minerals*, **13**(1), article 104, https://doi.org/10.3390/min13010104.

Wälle, M. & Wang, H.A.O. 2023. "Direct" thorium-lead dating of gem quality corundum by laser ablation ICP-TOF-MS. *EuroAnalysis XXI*, Geneva, Switzerland, 64–65, https://tinyurl.com/3uxhwnfn.

Wang, H.A.O., Krzemnicki, M.S., Chalain, J.-P., Lefèvre, P., Zhou, W. & Cartier, L. 2016. Simultaneous high sensitivity trace-element and isotopic analysis of gemstones using laser ablation inductively coupled plasma time-of-flight mass spectrometry. *Journal of Gemmology*, **35**(3), 212–223, https://doi.org/10.15506/JoG.2016.35.3.212.

Wang, H.A.O., Krzemnicki, M.S., Büche, S., Schmid, R. & Braun, J. 2019. Multi-element analysis of gemstones and its applications in geographical origin determination. *36th International Gemmological Conference*, Nantes, France, 28–31 August, 176–178, https://tinyurl.com/mt22x26w.

Wathanakul, P., Atichat, W., Pisutha-Arnond, V., Win, T.T. & Singbamroong, S. 2004. Evidences on the unusually high Be, Sn, Nb, and Ta content in some trapiche-like sapphires from basaltic origin. *29th International Gemmological Conference*, Wuhan, China, 2–18 September, 114–118.

Wathanakul, P., Atichat, W., Leelawattanasuk [*sic*], T., Sriprasert, B., Pisutha-Arnond, V., Sutthirat, C. & Win, T. 2007. The presence of beryllium and incompatible high field strength elements in some natural sapphires. *30th International Gemmological Conference*, Moscow, Russia, 15–19 July, 129–130.

Zhou, W., Krzemnicki, M.S. & Wang, H. 2024. Trace element in blue sapphire: Challenge or potential of element analyses by LA-ICP-TOF-MS for origin determination? *37th International Geological Congress (IGC 2024)*, Busan, Korea, 25–31 August, 2317–2318, https://tinyurl.com/2km9xbbk.

The Author(s)

Dr Michael S. Krzemnicki FGA[1,2], Dr Laurent E. Cartier FGA[1,3], Dr Wei Zhou FGA[1], Pierre Lefèvre[1], Dr Markus Wälle[1], Dr Hao A. O. Wang FGA [1] and Judith Braun[1]

[1] Swiss Gemmological Institute SSEF, Aeschengraben 26, 4051 Basel, Switzerland

[2] Department of Environmental Sciences, University of Basel, Bernoullistrasse 32, 4056 Basel, Switzerland

[3] Faculty of Geosciences and Environment, University of Lausanne, UNIL-Mouline Géopolis, 1022 Lausanne, Switzerland

Email: michael.krzemnicki@ssef.ch

Acknowledgements

The authors thank Rajesh and Kunal Sheth (House of Gems Ltd, Hong Kong), Raju Kothari (Kothari Trading Co. Ltd, Hong Kong), Alexander Leuenberger (Aline GmbH, Switzerland), Joseph Belmont (KV Gems, Bangkok, Thailand), Charles Abouchar (Abouchar SA, Geneva, Switzerland) and Frédéric Torroni (F. Torroni SA, Geneva) for the loan of sapphire samples used in this study. We are also grateful to our colleagues at SSEF—in particular L. Phan and A. Chalain of the photography department, and S. Büche, G. Brombach and M. Eland of the analytics department—for their valuable assistance. Finally, we thank Dr Walter Balmer (Balmer Collection, Switzerland) for insightful discussions and valuable input on the FTIR spectra of corundum.

An initial draft of this article was polished by ChatGPT. The authors reviewed, edited and revised the ChatGPT-edited text, and take ultimate responsibility for the contents of this publication.